Supporting information

Self-assembled tetraoctylammonium bromide as an electron-injection layer for cathode-independent high-efficiency polymer light-emitting diodes

Sung-Nien Hsieh [a)], Shih-Wei Hsiao [a)], Tsan-Yao Chen [d)], Chen-Yan Li [a,b)], Chih-Hao Lee [d,e)], Tzung-Fang Guo [b,c)], Yao-Jane Hsu [c,e)], Tsang-Lang Lin [d)], Yen Wei [f)], and Ten-Chin Wen [a)*]

[a)] Department of Chemical Engineering,
National Cheng Kung University,
Tainan 70101, Taiwan
[b)] Advanced Optoelectronic Technology Center,
National Cheng Kung University,
Tainan 70101, Taiwan
[c)]Institute of Electro-Optical Science and Engineering,
National Cheng Kung University,
Tainan 70101, Taiwan
[d)]Department of Engineering and System Science,
National Tsing-Hua University,
Hsinchu 30013, Taiwan
[e)]National Synchrotron Radiation Research Center,
Hsinchu 30076, Taiwan,
[f)]Department of Chemistry, Tsinghua University,
Beijing 100084, China

*Corresponding author

E-mail: tcwen@mail.ncku.edu.tw

Table S1 . Device performances of PLEDs with various cathode materials in a device configuration of glass/ITO/PEDOT:PSS/G-PF/cathode.

Cathode	$V_{L\text{-}on}$ [a] (V)	V [b] (V)	Brightness [b] (cd/m^2)	η [b] (cd/A)	Brightness [c] (cd/m^2)
Al	2.9	7.0	80	0.5	530
NH_4Br/Al	3.2	5.6	70	0.4	290
TEAB/Al [d]	2.6	6.2	600	3.5	2.88×10^3
TOAB/Al [d]	2.2	3.7	2.74×10^3	15.4	5.63×10^4
THAB/Al [d]	2.1	6.5	2.29×10^3	13.1	1.19×10^4
MTOAB/Al [d]	2.2	4.3	2.73×10^3	14.9	4.81×10^4
TMOAB/Al [d]	2.3	4.7	2.40×10^3	13.5	2.96×10^4
TBATPB/Al [d]	2.5	6.3	1.11×10^3	6.5	6.16×10^3

[a] $V_{L\text{-}on}$: Brightness at 1 cd/m^2.
[b] Device performance at a current density of 17 mA/cm^2.
[c] Brightness at 8 V.
[d] tetraethylammonium bromide (TEAB); tetraoctylammonium bromide (TOAB); tetrahexadecylammonium bromide (THAB); methyltrioctylammonium bromide (MTOAB); trimethyloctylammonium bromide (TMOAB); tetrabutylammonium tetraphenylborate (TBATPB).

In this experiment, various ammonium salts were used as the electron-injection layer (EIL). From Table S1, the ammonium salts with *n*-alkyl chains effectively reduced the electron-injection barrier between Al and G-PF to improve device performance. The best performance was obtained for the TOAB/Al-based device. However, the NH_4Br/Al-based device exhibited very poor performance. This result shows that the alky chains play an important role in the electron-injection ability of polymer light-emitting diodes (PLEDs). The relationship between the structure of the ammonium salts and the electron-injection ability is currently under investigation.

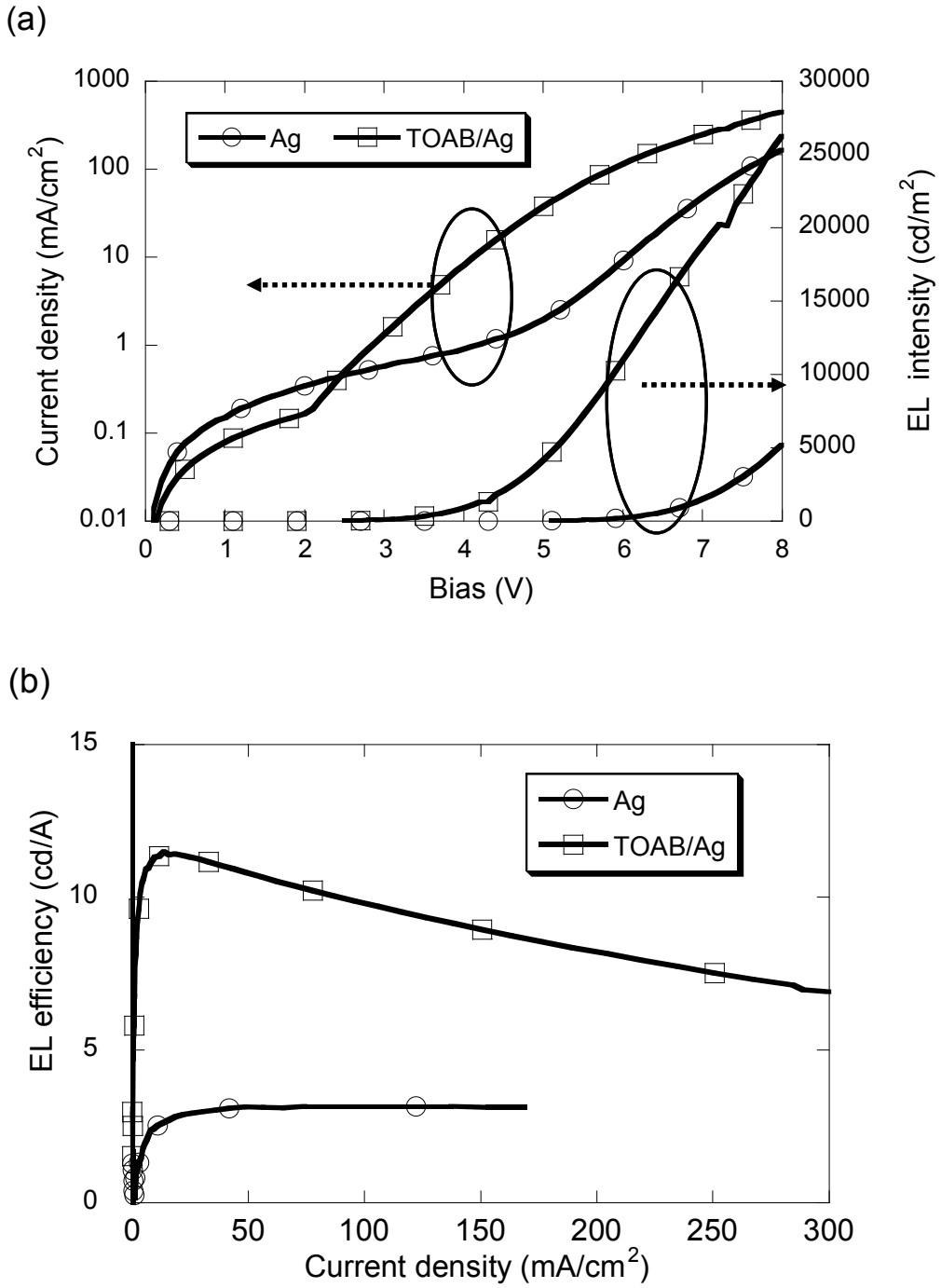

Figure S1. (a) *J-V-L* characteristics of devices with Ag and TOAB/Ag as the cathode and (b) corresponding EL efficiency vs *J* curves.

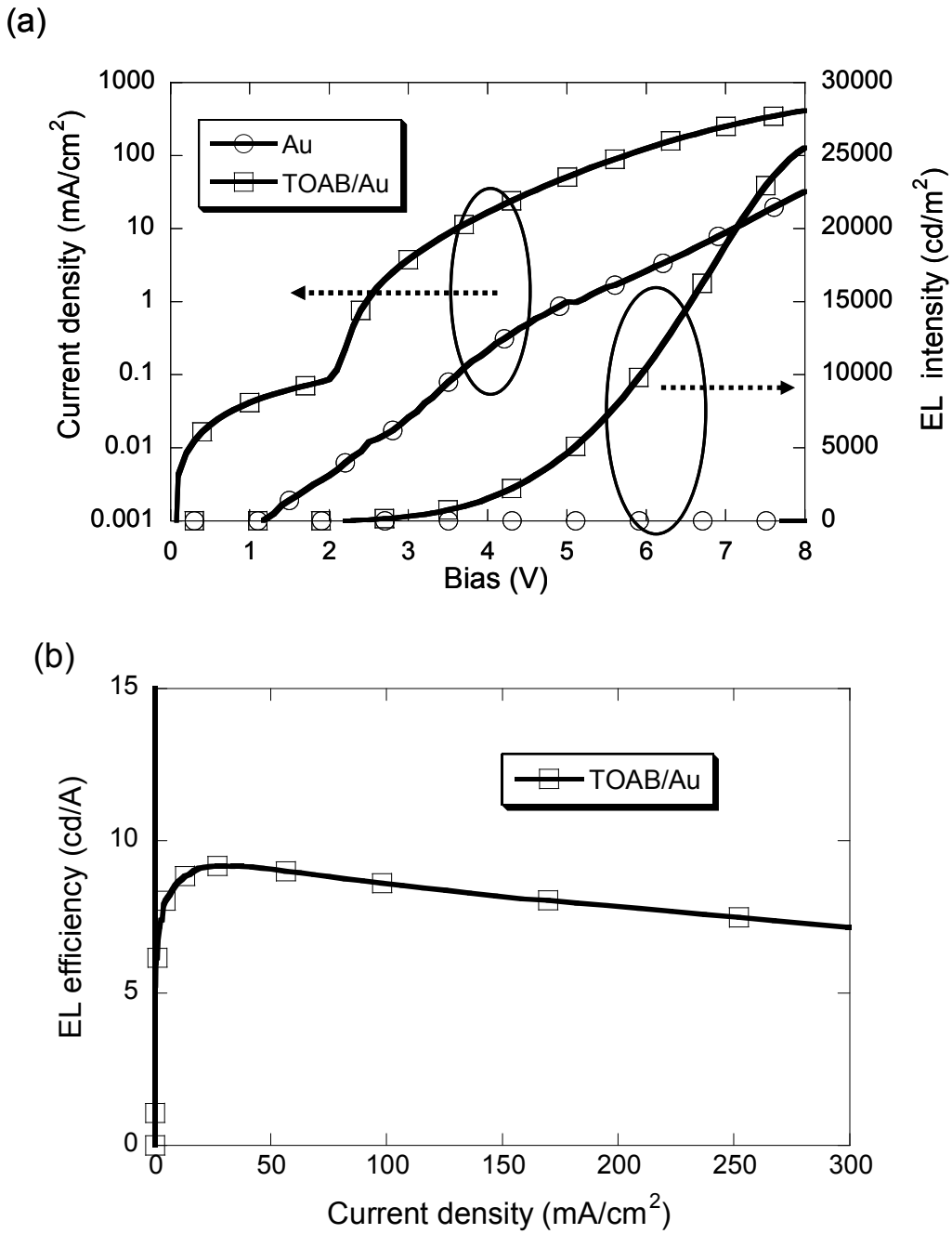

Figure S2. (a) *J-V-L* characteristics of devices with Au and TOAB/Au as the cathode and (b) corresponding EL efficiency vs *J* curves.

(a)

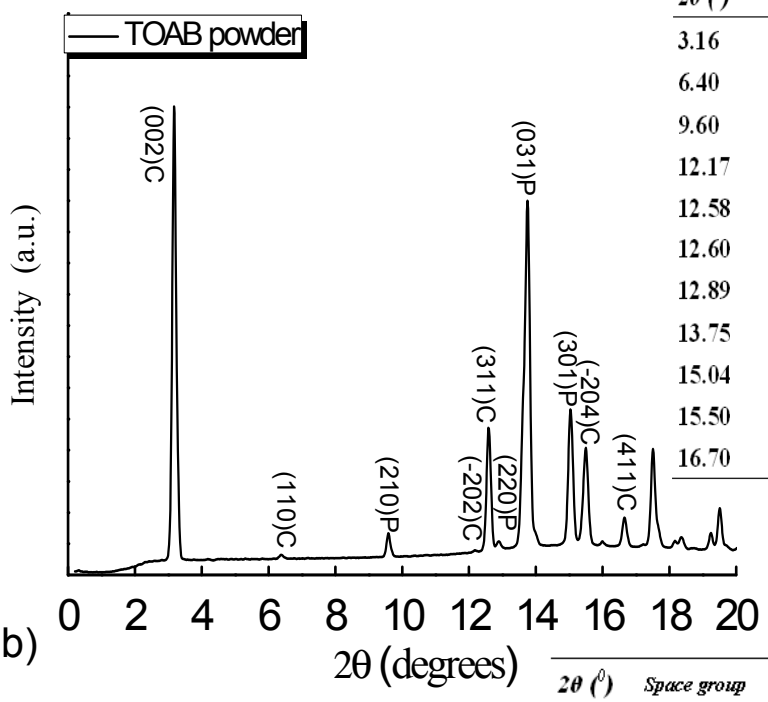

2θ (°)	Space group	index	D (μm)
3.16	C2/c	(002)C	0.719
6.40	C2/c	(110)C	0.346
9.60	$P2_1/n$	(210)P	0.258
12.17	C2/c	(-202)C	0.104
12.58	C2/c	(311)C	0.174
12.60	$P2_1/n$	(220)P	0.179
12.89	$P2_1/n$	(220)P	0.192
13.75	$P2_1/n$	(031)P	0.113
15.04	$P2_1/n$	(301)P	0.136
15.50	C2/c	(-204)C	0.126
16.70	$P2_1/n$	(411)C	0.126

(b)

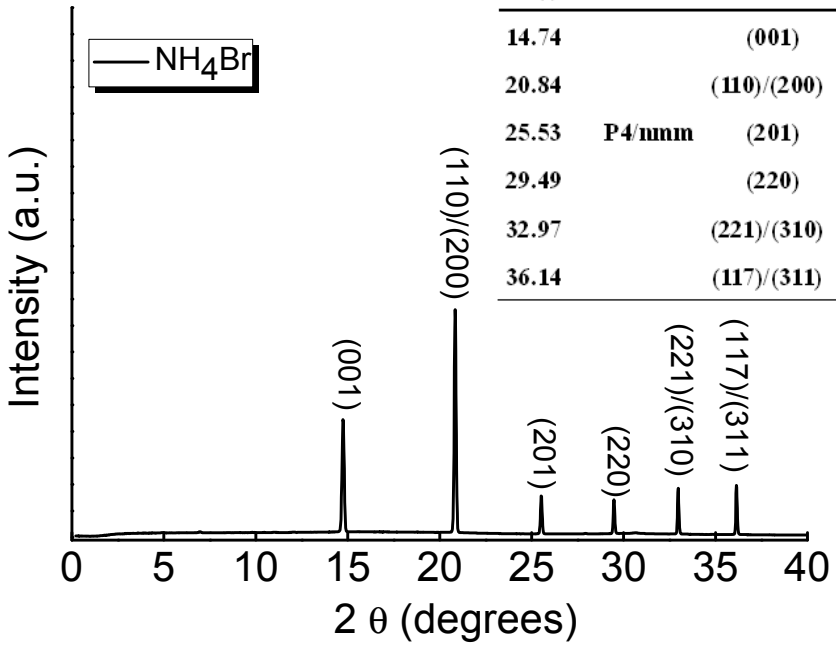

2θ (°)	Space group	index	D (μm)
14.74		(001)	0.172
20.84		(110)/(200)	0.135
25.53	P4/nmm	(201)	0.131
29.49		(220)	0.123
32.97		(221)/(310)	0.114
36.14		(117)/(311)	0.106

Figure S3. XRD profiles for powders of (a) TOAB and (b) NH_4Br. Data were collected in transmission mode using an X-ray wavelength of 1.02695 Å at beamline BL-01C of

National Synchrotron Radiation Research Center (NSRRC), Taiwan. The average coherent length (grain size, D) for the two powders on the corresponding lattice space was estimated using the Scherrer equation.

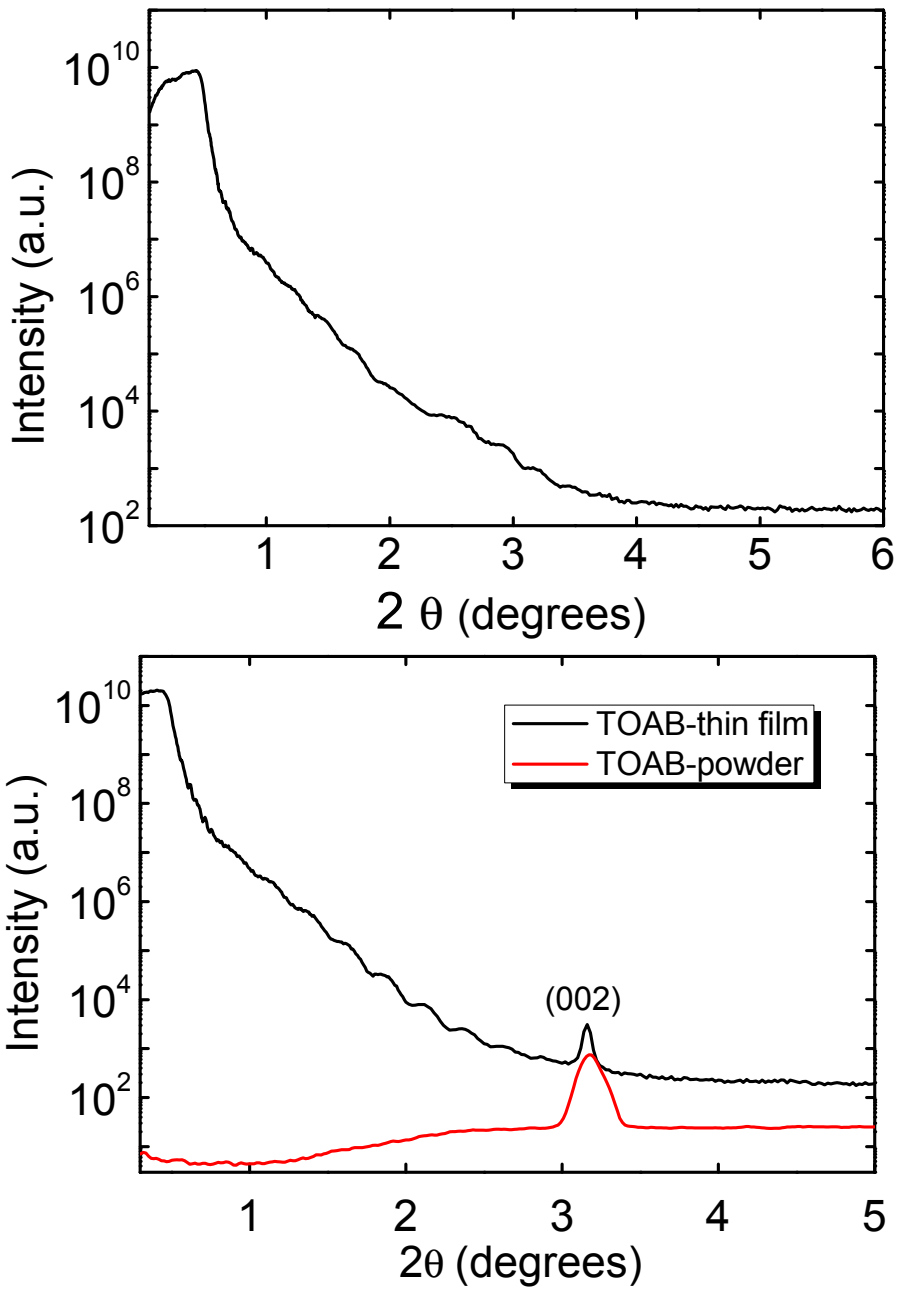

Figure S4. (a) Plane-normal synchrotron XRD pattern of the film for ITO/PEDOT:PSS/G-PF. (b) XRD patterns for ITO/PEDOT:PSS/G-PF/TOAB thin film and the powder of TOAB.

The XRD profile of TOAB powder with lattice indexes on the framework of the monoclinic phase is shown in Figure S3a[S1]. The EIL in this work is a polycrystalline TOAB powder comprising two types of monoclinic space group (C2/c and $P2_1/n$). The indexes were obtained by iterating the structure parameters (lattice space [d_{hkl}], lattice constants [a, b, and c], and lattice included angles [α, β, and γ]) of TOAB powder based on the monoclinic lattice equation (eq-S1):

$$\frac{1}{d_{hkl}^2} = \frac{h^2}{a^2 \sin^2 \beta} + \frac{k^2}{b^2} + \frac{l^2}{c^2 \sin^2 \beta} - \frac{2hl \cos \beta}{ac \sin^2 \beta} \quad \text{...S1}$$

In addition, the distributions of an average coherence length (grain size, D) with corresponding lattice spacings were estimated from XRD measurements. The D values are listed in the inset of Figure S3a. The most intense XRD peak and the biggest grain size for TOAB powder were contributed from C2/c along (002). The above results indicate that the preferential arrangement for TOAB molecules in the powder form is C2/c along (002). The preferential growth of TOAB crystallites with C2/c symmetry can be explained by the formation of a multilayer structure with a lattice plane consisting of horizontally arranged Br atoms with an inter-planar spacing of 18.6 Å, which is consistent with results of a model simulation and a diffraction analysis on single crystals[S1].

Figure S3b shows the XRD profile of NH_4Br powder. The NH_4Br crystallites were

indexed as the tetragonal phase in a P4/nmm symmetry. The indexes were obtained by iterating the structure parameters of NH_4Br powder based on lattice symmetries with the consideration of atomic scattering structure factors:

$$\frac{1}{d_{hkl}^2} = \frac{h^2 + k^2}{a^2} + \frac{l^2}{c^2} \quad \text{.....S2}$$

The distribution of the coherent length with corresponding lattice spacings is summarized in the inset of Figure S3b. The result indicates that NH_4Br grew into 3-dimensional homogenous crystallites (with average coherent lengths of around 0.1 - 0.2 μm) without directional preference. Accordingly, we can rule out the formation of a multilayer structure on NH_4Br considering that the long range periodic signal is absent in tetragonal crystallites.

Powder diffraction results can be used to determine the crystal structure for spin-coated TOAB thin film on G-PF. The first diffraction peak of TOAB thin film (see Figure S4b) appears at 3.16^{o} with a strong intensity, indicating that the preferential growth of TOAB thin film along the (002) lattice spacing is identical to that of powder crystallites. The full width at half maxium (FWHM) for the first diffraction peak of crystallites on TOAB film corresponds to an average grain size of 1.94 μm, which is 1.7 times larger than that of crystallites on TOAB powders. Such preferential growth can be rationalized by the presence of a heterogeneous surface (a noncrystalline hydrophobic PF surface) that reinforces the plane-normal growth of crystals with coincident direction which follows the preferential growth nature of TOAB molecules along (002). Further evidence is given by the rocking curve shown in the inset of Figure 6.

Table S2. XRR fitting parameters for glass/ITO/PEDOT:PSS/G-PF/TOAB sample.

Layer	Thickness (Å)	Scattering length density $\times 10^{-6}$ (Å)	Roughness (Å)
TOAB-top interface (1)	9.9	3.0	3.3
TOAB (2)	77.5	11.0	7.6
G-PF (3)	1011.8	9.4	12.1
PSS (4)	133.2	9.3	2.2
PEDOT (5)	221.2	11.0	6.2
ITO-PEDOT:PSS interface (6)	43.8	19.7	8.0
ITO (7)	923.7	53.4	15.0
Glass-ITO interface (8)	19.4	53.4	5.8

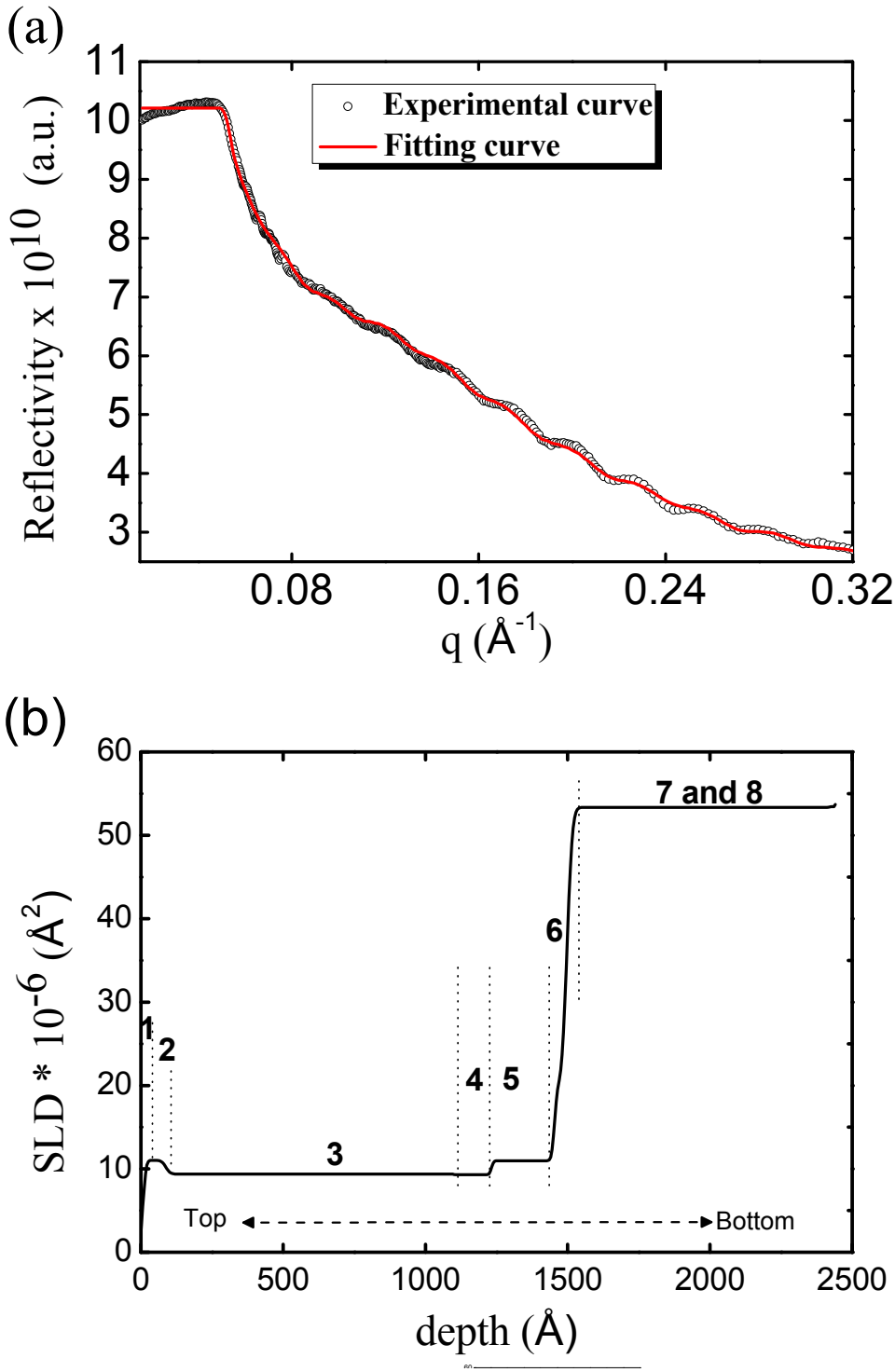

Figure S5. (a) XRR pattern of film for glass/ITO/PEDOT:PSS/G-PF/TOAB and its fitting curve. (b) Fitted scattering length density profile for glass/ITO/PEDOT:PSS/G-PF/

TOAB. In order to determine the thickness of TOAB on G-PF, X-ray reflectivity (XRR) measurements were performed. The diffraction/scattering experiments were conducted using a Huber 4-Circle Goniometer equipped with a Bicorn detector at wiggler beamline BL-13A of the NSRRC with an incident X-ray wavelength of 1.02695 Å. All spectra were recorded in the scattering vector (q) range of 0.004 to 0.31 Å ($q = 4\pi\sin\theta/\lambda$, where θ is the incidence angle, and λ is the wavelength of incident X-rays) and fitted with various layer models using the IGOR Pro 6.0 software package. The XRR fringe pattern for glass/ITO/PEDOT:PSS/G-PF/TOAB is shown in Fig. S5a. The IGOR Pro 6.0 (with a Motofit macro) formalism was adopted for recursive least-squares curve fitting, with each constituent layer parameterized with its thickness, root-mean-square roughness, and scattering length density (SLD). The SLD information for ITO, PEDOT, and PSS was obtained from Ref. S2. The SLD values for G-PF and TOAB were calculated by inputting their molecular formulas and densities into a theoretical estimation in the IGOR program. The model of a TOAB-coated PLED device was constructed in 8 layers comprising ITO, PEDOT, PSS, G-PF, and TOAB from bottom to top; 3 interfacial layers were inserted to express the interlayer structure diffusions modulating the SLD distributions between glass – ITO, ITO – PEDOT, and TOAB – air. The detailed parameters are listed in Table S2 and the XRR fitting curve is shown in Fig. S5a. The SLD profile of the fitted model is shown in Figure S5b. The thicknesses were estimated as 923.7 Å, 354.4 Å, 1011.8 Å, and 77.5 Å for ITO, PEDOT:PSS, G-PF, and TOAB, respectively. The best fit is presented. The film thicknesses for ITO, PEDOT:PSS, and G-PF were verified as 969 Å, 320 Å, and 960 Å, respectively, using a Tencor Alpha-Step 500 surface profiler.

(a)

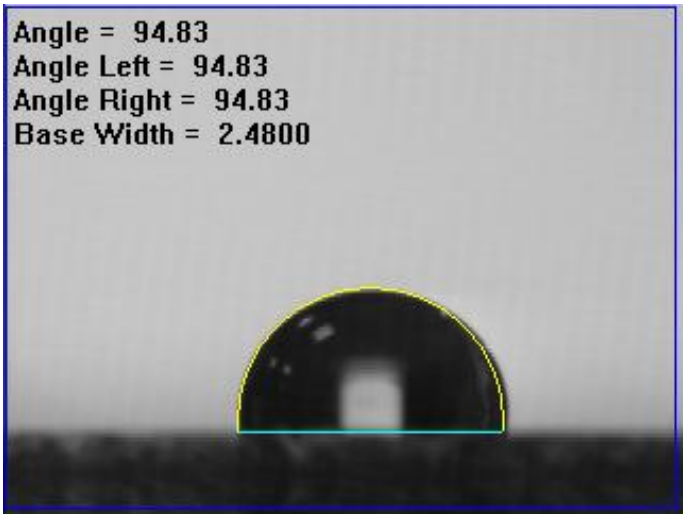

(b)

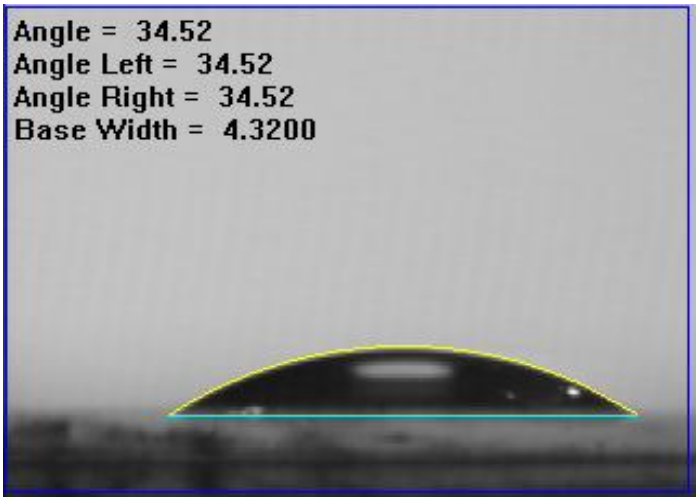

Figure S6. Optical photograph of a water droplet on (a) hydrophobic G-PF surface (water contact angle = 94.83^{o}) and (b) hydrophilic ZnO surface (water contact angle = 34.52^{o}). The contact angle measurements were performed using a contact angle instrument equipped with an image analysis attachment (First Ten Angstroms, Model FTA 100, USA). Distilled water was used as the probe liquid. Uniform drops of the liquids (2ul/drop) were carefully deposited on the sample surface using an assembly consisting of a micrometer syringe.

Table. S3 Device performance of PLEDs obtained using various TOAB solution concentrations in a device configuration of glass/ITO/PEDOT:PSS/G-PF/TOAB/Al.

Concentration (wt%)	$V_{L\text{-}on}$ [a] (V)	V [b] (V)	Brightness [b] (cd/m^2)	η [b] (cd/A)	Brightness [c] (cd/m^2)
0.05	2.3	4.1	2.80×10^3	14.8	4.86×10^4
0.1	2.2	3.6	2.60×10^3	14.3	4.92×10^4
0.2	2.2	3.7	2.74×10^3	15.4	5.63×10^4
0.3	2.2	3.6	2.65×10^3	13.4	3.97×10^4
0.4	2.3	3.6	1.85×10^3	13.2	3.47×10^4

[a] $V_{L\text{-}on}$: Brightness at 1 cd/m^2.
[b] Device performance at a current density of 17 mA/cm^2.
[c] Brightness at 8 V.

The TOAB thickness greatly affects device performance. Because the TOAB thickness can be controlled by varying the TOAB solution concentration, the concentration of the 2-methoxyethanol solution used to deposit the TOAB layer was varied from 0.05 to 0.4 wt%. A solution containing the ionic salt was spin-coated onto the surface of G-PF at 8000 rpm for 60 s and then the film was baked at 100 ^oC for 10 minutes. The device characteristics are summarized in Table S3. The optimal device performance was obtained with 0.2 wt%. At this concentration, the EL intensity of the TOAB/Al device biased at 8 V was 5.63×10^4 cd/m^2 and the maximum EL efficiency was 15.4 cd/A at 3.7 V and 2.74×10^3 cd/m^2. Therefore, this concentration was used to fabricate the device that was analyzed in this work.

References

S1 D. J. Abdallah, R. E. Bachman, J. Perlstein, R. G. Weiss, *J. Phys. Chem. B*, 1999, **103**, 9269.

S2 J. W. Andreasen, S. A. Gevorgyan, C. M. Schlepütz, F. C. Krebs, *Solar Energy Materials and Solar Cells.*, 2008, **92**, 793.